JOURNAL OF OPTOELECTRONICS AND ADVANCED MATERIALS Vol. 8, No. 1, February 2006, p. 271 - 279

# Numerical simulation of ohmic heating in idealized thin-layer electrodeposition cells

P. BARVINSCHI
*West University of Timisoara, Faculty of Physics, Bvd. V.Parvan 4, 300223, Timisoara, Romania*

The ohmic (Joule) heating in an electrolysis cell during electrochemical deposition (ECD) with a binary electrolyte could be significant since the conductivity of the solution without supporting electrolyte is low. Here we report some results concerning the simulation of the thermal field due to ohmic heating in idealized 2D and 3D thin-layer ECD cells. The mathematical model is based on a Laplace-type equation for the electrical potential and a time-dependent equation for the heat conduction. The coupled equations system is solved using a finite element method. The numerical results are compared with experimental ones and a qualitative agreement is found.

(Received December 15, 2005; accepted January 26, 2006)

*Keywords:* Thin-layer electrodeposition, Thermal field, Finite element method

## 1. Introduction

In electrochemical systems heat may be generated due to mass-transport phenomena and chemical reactions [1]. The combined set of gradients and of heat- and mass-transfer rates are coupled and they could modify the local properties within a given phase of the system and, as a consequence, they are influencing the course of some phenomena or the results of some properties measurements and their interpretation.

In a region of complex chemical composition like a thin-layer electrodeposition cell the mentioned effects may be even more important because in such a small volume the electric potential, density or temperature gradients, respectively, could have very large values. It is known also that in thin-layer ECD cells branched aggregates of qualitatively distinct morphologies are observed as the deposition parameters are varied [2]; is also important to establish the role of thermal effects in the morphology selection.

We have found only two references devoted to some features of thermal effects in thin-layer ECD. In the first one [3] there is a mention on the concentration measurement error due to temperature variation in an interferometric studies of branched electrodeposition. The other paper [4] is entirely devoted to an experimental study of the ohmic heating influence on the flow field in thin-layer ECD. In [4] a thin-layer ECD cell was filled with an $ZnSO_4$ aqueous solution and the electrodeposition was performed at a constant electrical potential. The deposit at the cathode was belonging to the homogenous or dense branched morphology (DBM). The temperature field due to Joule heating in the electrolyte solution was measured by means of an infrared camera. As mentioned in [4], the direct comparability of the results reported in this work with experiments performed in standard ECD cells is not possible because the ECD cell was of a slightly modified type. However, some of the results reported in [4] are appropriate to our purpose. These results are presented in figures 2 - 4 of the mentioned reference, giving an example of a two-dimensional thermography in the neighborhood of the anodic zinc wire, and the temporal evolution of the temperature field at the cathode and the anode as a function of the distance to the electrodes, respectively. The properties of the temperature field correspond closely with those of the concentration field in the cell (see bellow) and this observation motivate our approach.

A detailed description of the dense morphology in parallel geometry electrodeposition can be found in Ref. [5]. In this type of growth the electrodeposit consist in an array of quasi-regularly spaced porous trees (branches or filaments), as is shown in Fig. 1. This dense branched aggregate is bounded by a flat linear front which invades the cell at constant velocity and remains parallel to the electrodes. In the absence of convection and due to the fast electrodeposition of the cations near and between the tips, one can assume that the zone comprised between the cathode and the tips of the trees is totally depleted of cations. Correspondingly, the anions must be expelled from the tip region while the tip advance, otherwise they would create a large space charge region. The anions must leave this region at the same velocity as the front progress in the cell. The growth can thus be regarded as the advance of the front of an array of branches at a speed equal to the drift velocity of the anions; the growth front push away a depletion layer of both anions and cations (concentration boundary layer or diffusion layer) whose size remains constant. As the total amount of anions must remain constant the anions must accumulate near the anode, where their charge is balanced by anodic generation of an equal amount of cations, resulting a boundary layer of high concentration and low resistivity. Between the two boundary layers (cathodic and anodic) there is a neutral region whose concentration is equal to its initial value. The filaments are supposed to be highly conducting, therefore they keep the region between the cathode and the tips equipotential; the aggregate behave as a moving cathode.

The cathodic electrodeposition that belongs to the dense parallel morphology can be more or less regular. For high enough potential values, a regularly columnar or channel like deposit is formed [2,3].

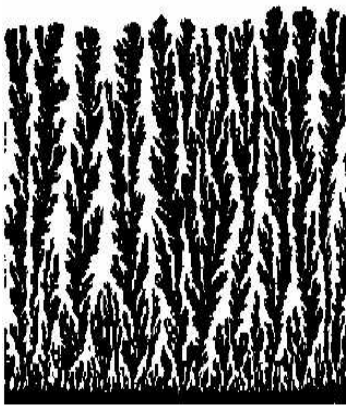

*Fig. 1. Illustration of dense growth by ECD in thin cell.*

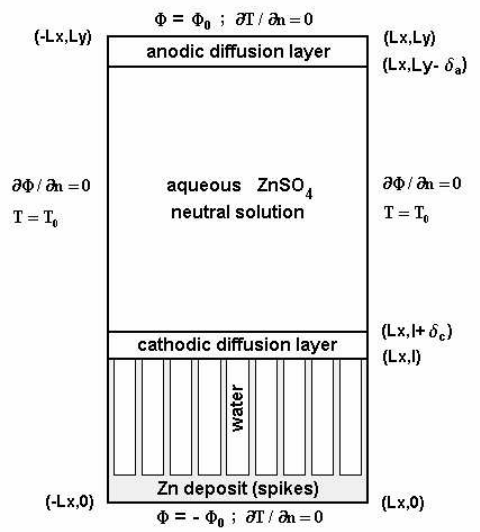


*Fig. 2. Schematic diagram of the problem space and the boundary conditions for the electrical and thermal problems.*

A macroscopic (>0.1 mm) characterization of a dense branched aggregate was proposed in [5]. The analysis relies on the computation of a correlation function which provides a statistical estimate of the mean distance $\lambda$ between branches and of the width *w* of the branches. If one defines the occupancy ratio $\theta$ as the proportion of the cell width occupied by the deposit then, in a first approximation, we can write $w = \theta\lambda$ and the deposit can be imagined as a rectilinear equally spaced set of filaments (see Fig. 2). Obviously, this approximation is very good for channel like deposits.

In this paper we present a model for the simulation of the thermal field in idealized 2D and 3D thin-layer ECD cells by solving the problem of simultaneous electric and time-dependent thermal conduction in two or three dimensions. The mathematical model is the same as in [6] but in the present work we extend the calculations to ramified deposits, making a rigorously parametric study of the temperature distribution in the ECD cells. The numerical results are compared with experimental measurements reported in [4] and we point out on some new results that could be useful in forthcoming studies devoted to this topics.

## 2. Theoretical and numerical model

In the following we present a numerical study of the temperature distribution in idealized 2D and 3D ECD cells solving the problem of combined electric and heat conduction. In our approach we consider only the contribution of the dissipated ohmic heat and neglect any other form of energy dissipation. In accordance with the description of the ECD process in section 1, we consider the active part of the electrochemical cell as a thin rectangular foil composed of two parallel electrodes made of the same metal (Zn), a dilute solution of a salt of this metal (in our case $ZnSO_4$), the electrodeposit and two diffusion layers, one in front of the deposit and the other near the anode. The electrodeposit is supposed to be of the same metal as the electrodes. In the idealized 2D cells the thickness of the foil lying in the *(x,y)* plane is supposed to be infinitesimally small. The more realistic 3D cell is composed of a finite thickness layer of the same electrolyte solution, two diffusion layers and a deposit sandwiched all of them between two parallel glass plates. The geometry of the thin layer in the *(x,y)* plane between the glass plates is the same as in the 2D case. The thickness of the 3D cell is measured in the *z* direction. Because the two electrodes are very thin and can conduct heat much better than the fluid and the glass, we assume that they have a negligible thermal resistance in both the *y*-direction and *z*-direction. As a result, the electrodes can be assumed to be transparent for the flux of heat and are removed from the model for the calculation of the temperature field.

Each numerical experiment is performed considering a fixed shape electrodeposit (no deposit growth). We consider the bulk solution and the two diffusion layers to be each of them homogeneous and at rest. It is assumed that electroneutrality is maintained in all the cell, and the diffusive and convective effects are absent. We focus on the study of the temperature distribution in such idealized 2D or 3D cells at a constant voltage applied between the two electrodes (potentiostatic conditions). Clearly, the model described so far is a first step toward a more realistic description of the ohmic heating in thin-layer electrodeposition, in which electroneutrality assumption is removed and full ion transport is taken into account. The analysis of the full problem will be carried out in a forthcoming paper.

Based on previous considerations we can calculate the temperature distribution in the electrochemical cell as follows. Supposing electro-neutrality holds and in the absence of diffusive and convective transport of charge carriers, each region of the solution in the cell behaves like

an ordinary metal and the electrical current density $\vec{j}$ flowing into the cell is related to the field strength $\vec{E}$ by

$$\vec{j} = \sigma\vec{E} = -\sigma\nabla\Phi \qquad (1)$$

where $\sigma$ is the electric conductivity and $\Phi$ is electric potential. Under the same conditions, the conservation of electrical charge requires that

$$\nabla \cdot \vec{j} = 0 \qquad (2)$$

Combining the relations (1) and (2) we obtain

$$\nabla \cdot \vec{j} = \nabla \cdot (-\sigma\vec{E}) = \nabla \cdot (-\sigma\nabla\Phi) = 0 \qquad (3)$$

This is a PDE of the Laplace type where the conductivity $\sigma$ may vary in space. The current density causes dissipation of heat at a rate $\vec{j} \cdot \vec{E}$ per unit volume. This electric power will appear as a source term $h$ in the time-dependent equation for heat conduction

$$\nabla \cdot \vec{f} + \rho c_p \frac{\partial T}{\partial t} = h \qquad (4)$$

where $T$ is the absolute temperature, $\vec{f} = -k\nabla T$ the heat flux density, $k$ the thermal conductivity, $\rho$ the mass density and $c_p$ the specific heat capacity. In order to calculate the temperature distribution in the ECD cell we must solve simultaneously equation (3) for the electrical potential and equation (4) for temperature with appropriate initial and boundary conditions.

Each region of the 2D or 3D cell is characterized by its own electrical and thermal conductivity, mass density and specific heat capacity. Some data are taken from [7] and [8] and all of them are summarized in Table 1. For the purpose of the present study these properties are assumed temperature invariant.

*Table 1. Physical and chemical property data.*

| | k $Wm^{-1}K^{-1}$ | σ $\Omega^{-1}m^{-1}$ | ρ $c_p$ $Jm^{-3}K^{-1}$ |
|---|---|---|---|
| Deposit (Zn) | 121 | $1.5 \times 10^7$ | $2.78 \times 10^6$ |
| Cathodic diffusion layer (0.001 M/l) | 0.6 | 0.005 | $4.0 \times 10^6$ |
| Neutral solution (0.1 M/l) | 0.4 | 0.456 | $4.5 \times 10^6$ |
| Anodic diffusion layer (0.25 M/l) | 0.6 | 10 | $4.6 \times 10^6$ |
| Glass plates | 0.78 | $10^{-11}$ | $2.268 \times 10^6$ |

The initial conditions are always $T$ = 300K for the temperature and $\Phi$ = 0 for the electrical potential. The boundary conditions are of Dirichlet and Neumann type and they must be specified only on the boundary separating the system and its surroundings: $\Phi = -\Phi_0$ and $\partial T/\partial n = 0$ on the cathode side, $\Phi = +\Phi_0$ and $\partial T/\partial n = 0$ on the anode side and $\partial\Phi/\partial n = 0$ and $T = T_0$ on the lateral boundaries of the cell, where $\Phi_0$ is half the voltage applied to the ECD cell and $\vec{n}$ is the outward normal at the boundary of the domain. For the 3D cell additional boundary conditions were specified on the external faces of the glass plates: for the lateral ones the conditions are the same as for the corresponding sides of the 2D cell, and for the bottom and up faces we put $\partial\Phi/\partial n = 0$ and $\partial T/\partial n = 0$. In our problem no boundary conditions are needed for $\Phi$ and T at the interfaces between two different regions because the program treat as continuous the electrical potential and the temperature across the interfaces.

In the case of Joule heating, there are a variety of possible electrode boundary conditions for the thermal problem. An inspection of the experimental temperature profiles shown in Figs. 3 and 4 of Ref. [4] may suggests that the thermal boundary conditions are changing in time. For example, we think that on the cathode side there is a first period when the boundary conditions must be of the Neumann type but with a non-vanishing value of the outward surface-normal flux $\partial T/\partial n$, followed by a regime when the boundary conditions are of the Dirichlet type ($T$ is some constant temperature). For the sake of simplicity, in our calculations we have adopted the mentioned boundary conditions but a study of other choices for this type of problem could be interesting.

For the numerical solution of the equations we have used the student version of the finite element PDE solver FlexPDE [10]. A 2D problem space is divided into triangular elements and the variables are approximated by second or third order polynomials; in a 3D problem the space is divided into tetrahedrons. The program employs an adaptive mesh refinement technique to improve the accuracy of the solution.

## 3. Results and discussion

### 3.1 Thermal field in idealized 2D cells

As a first approach to the analysis of the thermal field in simplified thin-layer ECD cells we take a 2D ramified deposit with ten equidistant spikes having a compact rectangular shape. The problem space is shown in Fig. 2. The length and width of the cell are the same in all numerical experiments, $L_y$ = 40 mm and $2L_x$ = 20 mm respectively. The distance between the axis of two successive spikes is $\lambda$ = 2 mm. Based on experimental findings concerning the homogeneous electrodeposition from $ZnSO_4$ aqueous solution, in our model we suppose that between spikes there is pure water. A number of parameters in the problem can be varied: the applied electric potential $\Phi_0$, the width $\delta_c$ and $\delta_a$ of the cathodic and anodic diffusion layers respectively, the physical properties of the regions in the cell ($\sigma$, $k$, $\rho$, $c_p$), the length $l$ and the width $w$ of the spikes in the deposit. We

are able than to make a parametric study of the ohmic heating phenomenon in our simplified ECD cells. We performed calculations for various values of $\Phi_0$ , $\delta_c$, $l$ and $w$; because the width of the cell has a constant value, changing $w$ means a variation of the occupancy ratio $\theta$. For $\theta = 1$ the spikes touch each other and the deposit becomes a compact one.

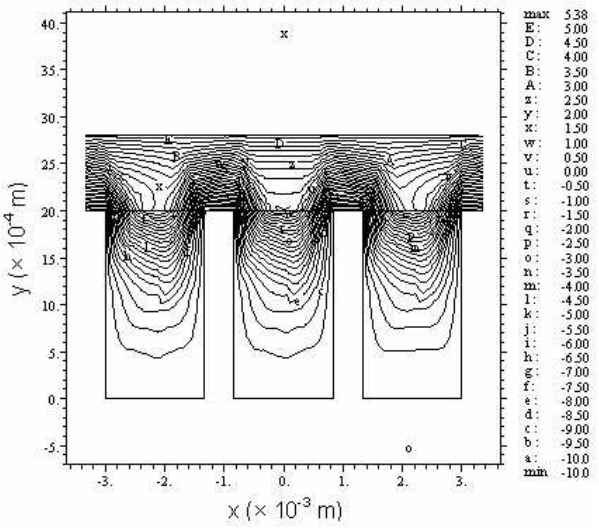


*Fig. 3. Equipotential lines for the solved electrical potential near the deposit; the values of the contours are given on the right in volts (see text for details).*

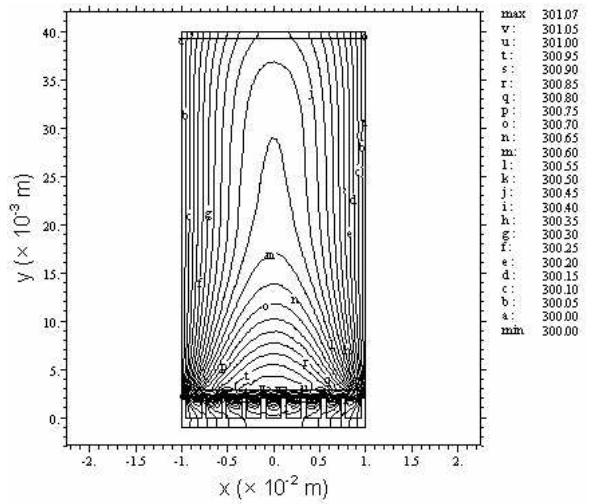


*Fig. 4. Isothermal lines for the calculated thermal field in the entire ECD cell arising from Joule heating; the values on the right are in Kelvin (see text for details).*

We have calculated the two-dimensional electrical potential $\Phi(x,y)$ and the electric field $\vec{E}(x,y)$ in the cell. A typical result for $\Phi(x,y)$ obtained for the values of parameters $l$ = 2 mm, $\Phi_0$ = 10 V, $\delta_c = \delta_a$ = 0.8 mm, $\theta$ = 0.73 at the moment $t$ = 400 s is shown in Fig. 3. We see that the equipotential lines are deformed in the usual manner due to the presence of spikes. The electric field (not shown here) is concentrated on the tips of spikes and almost vanish in the rest of the cell, having very small values between the spikes.

The calculated temperature distribution in the entire cell $T(x,y)$ for the same values of parameters as in Fig.3 is shown by contours lines in Fig. 4. A painted image of this temperature distribution resemble quite well the thermography in Fig. 2 of reference [4]. The temporal evolution of the temperature distribution along the $y$ direction in the cell, for the same values of parameters, is shown in Fig. 5. The general behavior of the simulated temperature distribution is qualitatively similar to that found experimentally and reported in Ref. [4] (see Figs. 3 and 4 of this reference), but the temperature increase is not the same. The most important features of the temperature profile is the existence of a local temperature maximum whose position correspond to that of the cathodic diffusion layer, followed by a plateau of spatially quasi-constant temperature extended in a region between the two diffusion layers.

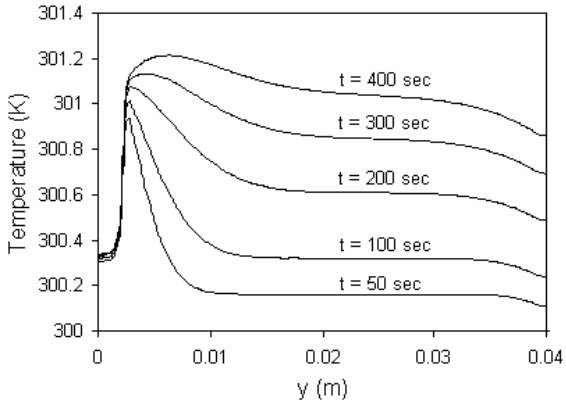


*Fig. 5. Calculated temperature profiles along the 2D cell (see text for the values of parameters).*

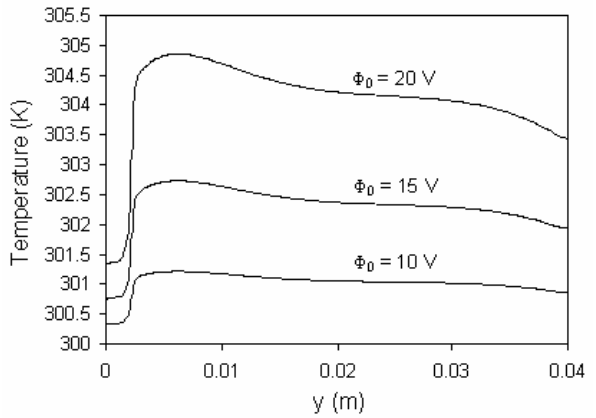


*Fig. 6. The dependence of the calculated temperature along the 2D cell on the voltage applied to the cell (see text for the values of the other parameters).*

We make a step further in our analysis focusing on the dependence of the temperature profile along the cell, $T(y)$, on some parameters involved in the model. First of all, one would expect an increase of the temperature in the entire cell as a result of an increase of the applied electric

potential $\Phi_0$. Our calculation show that this assertion is true, as one can see in Fig. 6 where we have represented the *T(y)* distribution for three values of $\Phi_0$ (10 V, 15 V, and 20 V) at t = 400 s and keeping all the other parameters at the same values ($l$ = 2 mm, $\delta_c = \delta_a$ = 0.8 mm, θ = 0.73). It is also remarkable that for various values of $\Phi_0$ the shape of the *T(y)* distribution is the same.

Turning out to the dependence of the temperature profile *T(y)* on the occupancy ratio θ, the result of the calculation for $l$ = 2 mm, $\Phi_0$ = 10 V, $\delta_c = \delta_a$ = 0.8 mm at t = 400 s and three values of θ (0.23, 0.60 and 1.00) are shown in Fig. 7a. Trying to explain this behavior of the temperature we have performed a calculation of the electrical potential *Φ(y)* along the cell for the same values of the parameters and the results are shown in Fig. 7b. There is a remarkable resemblance between the profiles in this figure and the profiles for the electric potential obtained by Chazalviel (see Figs. 2 and 3 in Ref. [9]). We observe that the most important part of the potential drop in the cell is confined in the very narrow region in front of the deposit (the cathodic diffusion layer). As is seen in Fig. 7b, a slightly dependence of *Φ(y)* with the occupancy ratio is observable for higher values of θ and a more important one for small values of θ. In our pure ohmic model this behavior of *Φ(y)* can be explained by the increase of the potential drop along the deposit as a result of an increasing of the electrical resistance when θ decrease. A motivation for the dependence of the temperature distribution *T(y)* on the occupancy ratio can now be offered. It is clearly seen that in the deposit region the temperature is higher for small values of θ and that in front of the cathodic diffusion layer the situation is reversed (the temperature increase for high occupancy ratio). These observations are in accord with the electrical potential dependence on θ discussed previously: the potential drop along the deposit is more important for small values of θ, and the temperature in this region will increase when θ decrease because the electrical power has the same behavior as the potential. In the same time, the potential drop in the bulk solution is increasing for higher values of θ, so the temperature in this region increases when the occupancy ratio increases too.

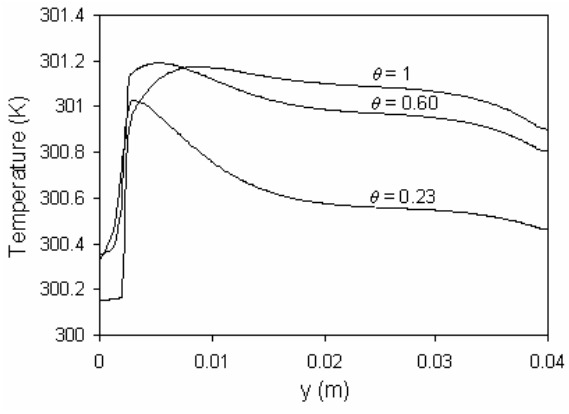


a

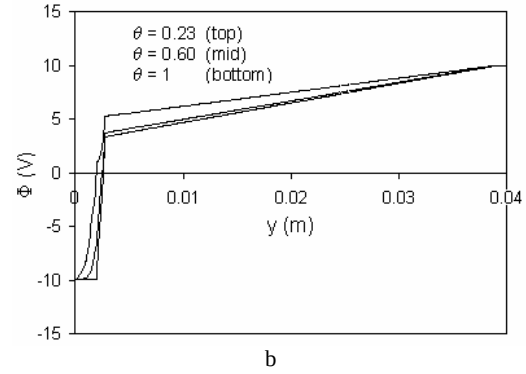


b

*Fig. 7. Dependence of the calculated temperature profile T(y) on the occupancy ratio θ (a), and the corresponding electrical potential profiles along the cell (b).*

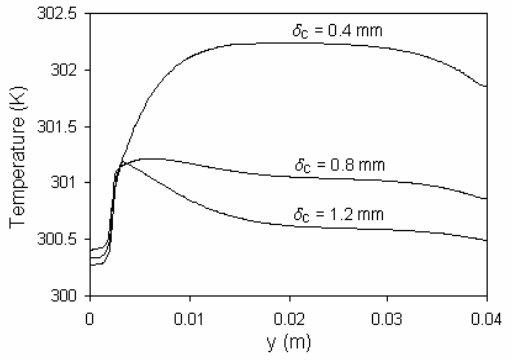


a

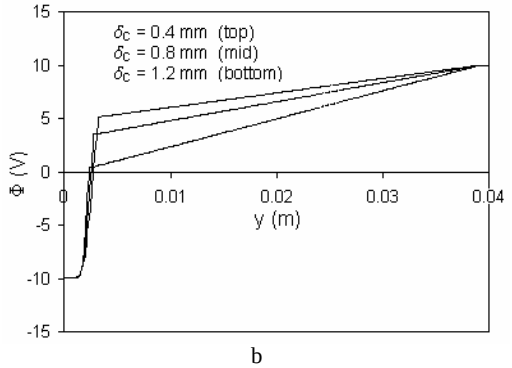


b

*Fig. 8. Dependence of the calculated temperature profile T(y) on the cathodic diffusion layer width $\delta_c$ (a), and the corresponding electrical potential profiles along the cell (b).*

Another clear effect on the temperature profile *T(y)* is due to the variation of the cathodic diffusion layer width $\delta_c$. The calculated *T(y)* profiles for $l$ = 2 mm, $\Phi_0$ = 10 V, $\delta_a$ = 0.8 mm, θ = 0.73 at $t$ = 400 s, for three values of $\delta_c$ (0.4 mm, 0.8 mm and 1.2 mm), are shown in Fig. 8a. The corresponding electrical potential profiles (Fig. 8b) give once again the motivation for the behavior of the temperature distribution in the cell: an increase of the potential drop in the bulk solution follows the reduction of the diffusion layer width and this implies an increase of the temperature in the bulk solution region.

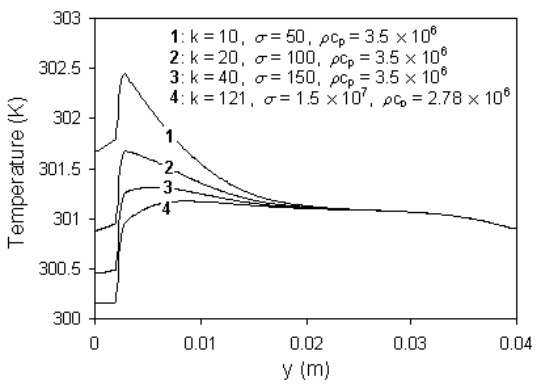


*Fig. 9. Dependence of the calculated temperature profile T(y) on σ, k and $\rho c_p$ in the deposit; the indicated values have the same units as in Table 1.*

As it is known, the density of metal in the electrodeposit region is very low (see section 1) and the previous assumption of homogeneous and compact pure metallic deposit is a very crude approximation. Despite the fact that the deposit is considered to have a very good electrical and thermal conductivity, we think that the appropriate average values for σ, *k*, ρ and $c_p$ for a kind of homogeneous and compact deposit are closer to those of an aqueous solution rather than those of a metal. For this reason we have performed a number of simulations taking for σ, *k* and ρ $c_p$ in the deposit region some fictitious values ranging between the corresponding ones for water and metallic zinc, the other parameters being the same: $l$ = 2 mm, $\Phi_0$ = 10 V, $\delta_c = \delta_a$ = 0.8 mm, θ = 1.00. The resulting *T(y)* profiles at t = 400 s are shown in Fig. 9. We see that the values of temperature in the deposit region are increasing if the values of σ and *k* become more and more closer to that of water. In the same time, the *T(y)* profile in the rest of the cell is roughly unchanged.

From the results presented so far it is clearly seen that he temperature profile along the cell, *T(y)*, has roughly the same shape whatever the θ may be, in other words for all morphologies belonging to he homogeneous growth. However, important differences between the shapes of the temperature profiles in the *x* direction (parallel to the growth front) are seen when we change the occupancy ratio and implicitly the morphology of the deposit. Such temperature distributions are shown in Figs. 10a – d for $l$ = 2 mm, $\Phi_0$ = 10 V, $\delta_c = \delta_a$ = 0.8 mm and three occupancy ratio (θ = 0.23, 0.60 and 1.00) at $t$ = 400 s. The *T(x)* profiles are calculated at the distances $y = l - \delta_c$, $y = l$, $y = l + \delta_c$ and $y = l + 2\delta_c$ from the cathode. These profiles suggest that important gradients of temperature may exist between the spikes and in the tip region. The possible influence of such temperature gradients on the cathodic convective rolls is a topic that will be carried out in a forthcoming paper. *T(x)* profiles calculated for different values of the cathodic diffusion layer width $\delta_c$, not shown here, conduct to similar results: when $\delta_c$ increase, *T(x)* decrease in the deposit area but increase in front of the deposit; as compared to the occupancy ratio influence, this time the temperature gradients are smaller.

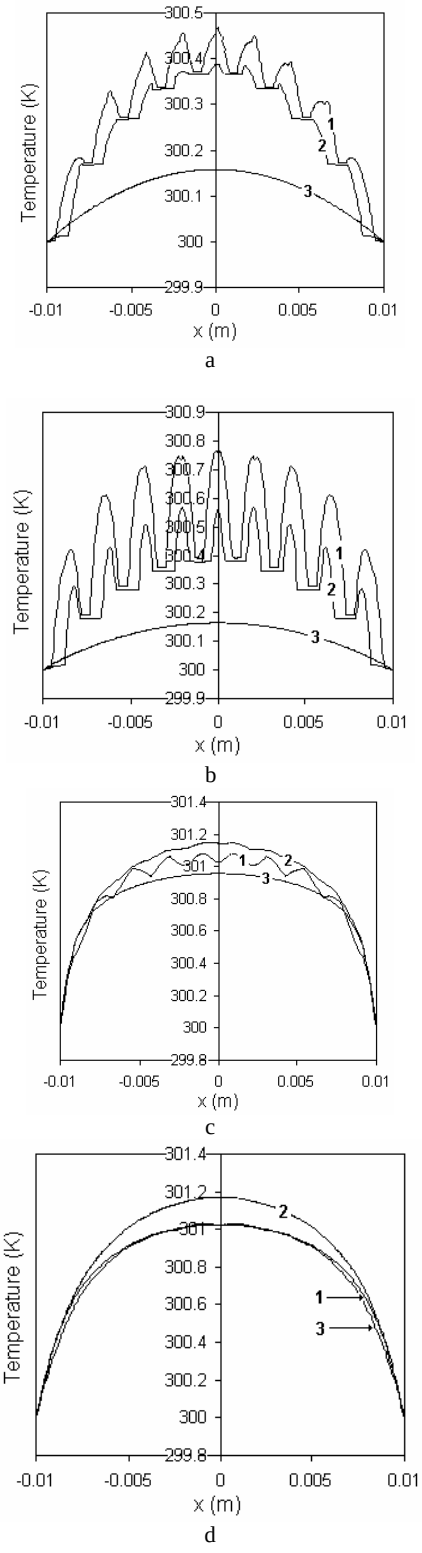


*Fig. 10. Calculated temperature profiles in the direction parallel to the growth front at the distances $y = l - \delta_c$ (a), $y = l$ (b), $y = l + \delta_c$ (c) and $y = l + 2\delta_c$ (d) from the cathode, for the occupancy ratio θ = 0.23 (1), θ = 0.60 (2), and θ = 1.00 (3). (See text for the other parameters).*

### 3.2 Thermal field in simplified 3D cells

We next consider the case of a more realistic ECD cell, composed of a thin layer of the same electrolyte, a metallic deposit (Zn) and two diffusion layers (cathodic and anodic) confined between two parallel glass plates. Due to the limited number of nodes in the student version of the FlexPDE program, the geometry of the thin layer between the glass plates in the *(x,y)* plane is very simple: the deposit is supposed to be a homogeneous and compact rectangle (occupancy ratio $\theta = 1$), having the length $l$ and the width $2L_x$. Because the study in the present work is a qualitative one and taking into account the results obtained in the previous section, the case $\theta = 1$ is appropriate for our purposes. We have performed the same numerical experiments as in the 2D cells but with two additional parameters, the thickness $t_w$ of the glass plates and the thickness $t_s$ of the solution between the plates.

The calculated electrical potential $\Phi(y)$ in the middle plane of the cell has the same profile as in the idealized 2D cells and is not shown here. In what follows we focus only on the temperature distribution in the cell and its dependence on some parameters involved in the problem. We begin by presenting the two-dimensional temperature distribution $T(x,y)$ in the middle plane of the cell and on the external side of the glass plate at $t = 400$ s (Fig. 11a and 11b), calculated for the parameters values $l = 3$ mm, $\Phi_0 = 10$ V, $\delta_c = \delta_a = 1.0$ mm, $t_w = 2$ mm and $t_s = 0.5$ mm. The temperature distribution $T(y,z)$ in the cross section of the cell for $x = 0$ and the same values of parameters is shown in Fig. 11c. More illustrative for our study are the profiles of the temperature distribution along the cell, $T(y)$, for some given $x$ and $z$ coordinates and different values of the parameters involved. We will consider the $T(y)$ profiles in the middle plane of the cell ($x = 0$, $z = t_w + t_s/2$) and on the external side of the glass plate ($x = 0$ and $z = 0$ or $z = 2t_w + t_s$).

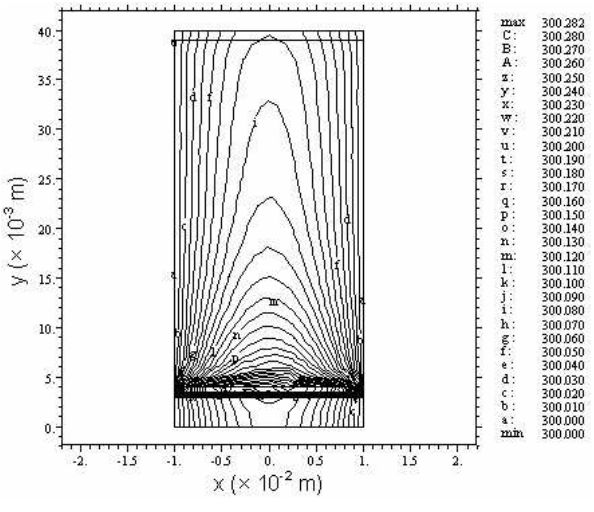


a

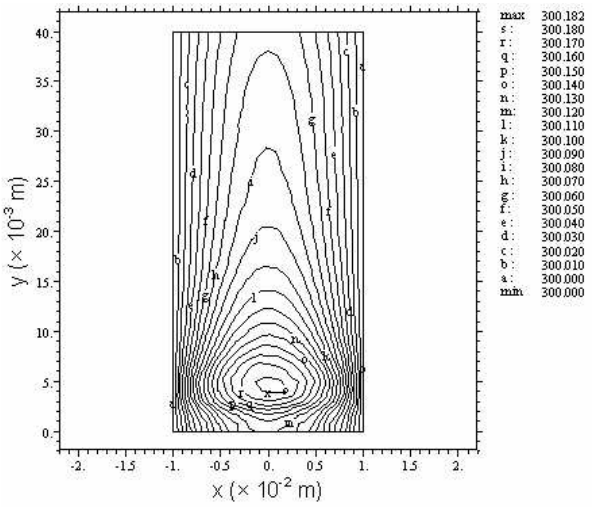


b

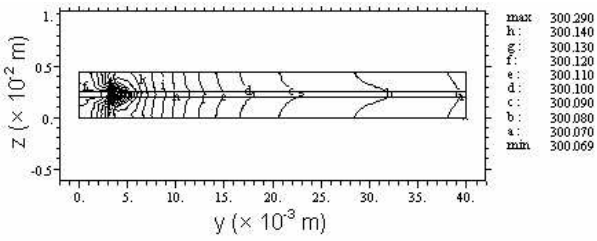


c

*Fig. 11. Isothermal lines for the calculated thermal field in the 3D cell in the middle plane of the cell (a), on the external side of the glass plate (b) and in a vertical cross section (c); the values on the right are in Kelvin. (See text for details).*

The calculated $T(y)$ profiles in our 3D cell for the same parameters as those in Fig. 11 are shown in Fig. 12, together with the $T(y)$ profile for the same values of $l$, $\Phi_0$, $\delta_c$, $\delta_a$ and at the same time but in the 2D cell with a compact deposit. First of all we observe that the $T(y)$ profile in the 3D cell has the same shape as in the 2D cell. Obviously, for the same values of the parameters the temperature in the 2D cell is higher than the temperature in the 3D cell because the electric power is the same but the heated volume is much larger in the case of 3D cell. We also observe an important difference in the values of the maximum temperature in the middle plane of the cell and on the external side of the glass plate. In the same time, we note that the shape of the $T(y)$ curves in the two planes of the cell are different for $y$ between 0 and roughly $l + 2\delta_c$ : as normal, the glass plate has a decreasing and smoothing effect on the temperature profile for the $y$ coordinate lying in this range. Due to this smoothing effect of the glass plate on the temperature profile, the resemblance between our calculated $T(y)$ profile in 3D cells and the corresponding experimental profile in Ref. [4] is better than in the case of 2D cells.

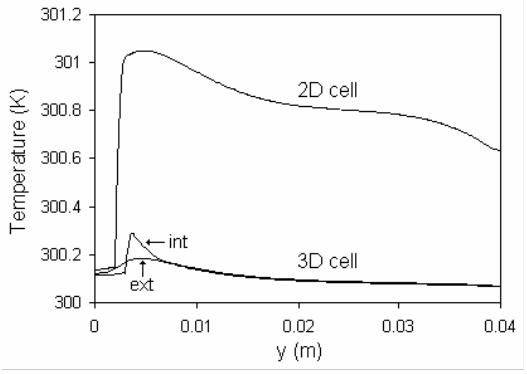


*Fig. 12. Calculated temperature profiles along the 2D and 3D cells; "int" and "ext" means the temperature in the middle plane of the cell and on the external side of the glass plate, respectively, in the 3D cell. (See text for details).*

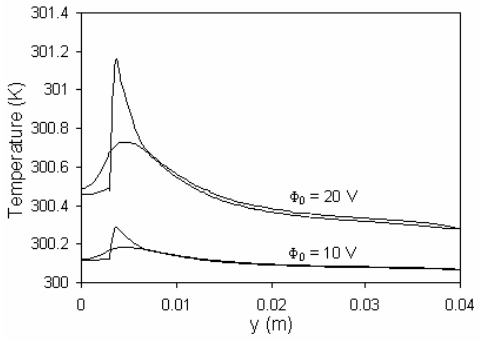


a

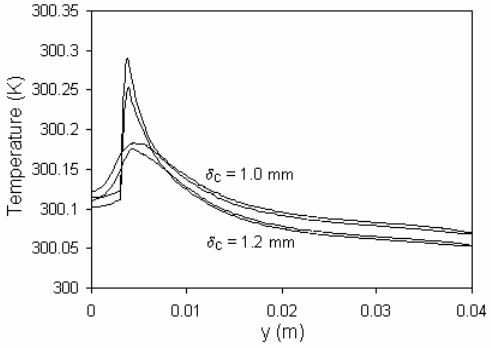


b

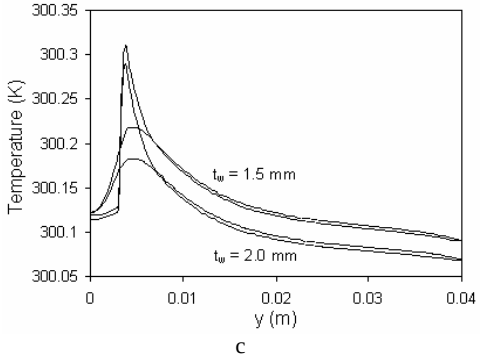


c

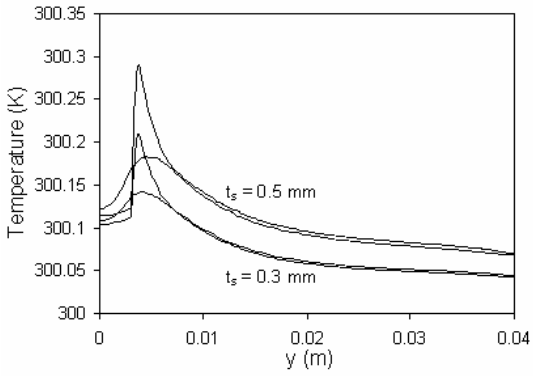


d

*Fig. 13. Dependence of the calculated temperature profiles along the 3D cell on the applied electrical potential (a), cathodic diffusion layer width (b), wall thickness (c), and electrolyte thickness (d).*

Other calculated *T(y)* profiles in the two planes of the 3D cell showing the dependence of temperature on $\Phi_0$ , $\delta_c$, $t_w$ and $t_s$ are presented in in Figs. 13a – d. Keeping at the same values all the other parameters and increasing only the applied electrical potential $\Phi_0$ , the electrical power becomes larger in the same volume and the temperature increases too, as is seen in Fig. 13a. The explanations for the temperature dependence on the variation of the cathodic diffusion layer width $\delta_c$ (Fig. 13b) is the same as in the case of 2D cell and we don't repeat them here. New facts in the case of 3D cell are the dependences of *T(y)* on the glass plates and solution thickness (Fig. 13c and 13d, respectively). For a constant value of the solution thickness and decreasing the glass plates thickness, the temperature in the entire cell is increasing. This can be easily understood: the heat source being the same, for a smaller volume of the system its temperature becomes higher. In the same time, the difference between the maximum temperature in the solution and on the external side of the glass wall is obviously smaller when $t_w$ decrease. We have an opposite situation when the solution thickness is decreased, keeping the same value for the glass plates: the electrical power density is the same but the volume of the heating source is smaller, so the temperature of the system decreases when $t_s$ is smaller.

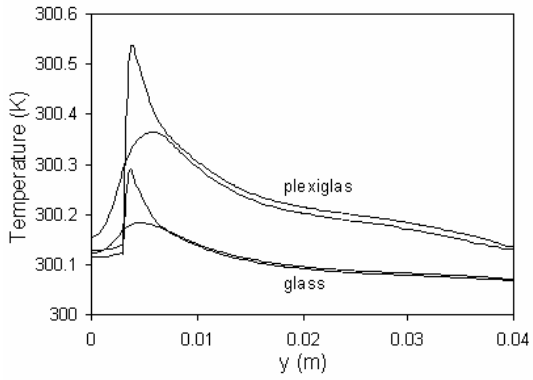


*Fig. 14. Comparison of the temperature profiles along two 3D cells having the walls made of glass and Plexiglas, respectively, the other parameters being the same (see text).*

We saved an very important observation for the end of this section: the *y* coordinate of the maximum temperature in the solution is always smaller than the *y* coordinate of the maximum temperature on the external side of the glass wall. A closer inspection of Figs. 12 - 13 reveals that the shift $\Delta y$ between the coordinates of the two maxima depend on the various parameters involved in the problem ($\Phi_0$, $\delta_c$, etc). Replacing glass with Plexiglas ($\sigma = 10^{-13}$ S m$^{-1}$, $k = 0.20$ W m$^{-1}$ K$^{-1}$, $\rho = 1190$ kg m$^{-3}$, $c = 1470$ J kg$^{-1}$ K$^{-1}$) of the same thickness, the shift $\Delta y$ is even larger, as is seen in Fig. 14. This fact can be understood comparing the thermal diffusion coefficient $a = k / \rho c_p$ for the media in the cell ($a$ is roughly $4.0 \times 10^{-7}$ m$^2$ s$^{-1}$ for glass, $1.0 \times 10^{-7}$ m$^2$ s$^{-1}$ for Plexiglas and $1.4 \times 10^{-7}$ m$^2$ s$^{-1}$ for water). Because the penetration time [11] varies as $1/a$, the existence of a difference between the position of the two temperature maxima and its dependence on material properties is easy to understand.

## 4. Conclusions

We have performed a numerical study of the ohmic heating in idealized 2D and 3D thin-layer electrochemical deposition cells. Based on experimental data, the domain used for the simulation is composed of four regions: deposit, cathodic diffusion layer, bulk electrolyte solution and anodic diffusion layer. We don't take into account the growth of the deposit and the transport of ions by diffusion and convection, our model being a static and pure ohmic one. The mathematical model consist of two PDE, a Laplace-type equation for the electrical potential and the time-dependent equation for heat conduction. They are simultaneously solved by the finite element method using a program called FlexPDE. We have computed the electrical potential, electrical field strength, electrical current density, and the temperature distribution in the entire 2D and 3D cells. We were able to made a parametric study of the temperature distribution, our results being confirmed by some experimental facts and pointing out on other aspects belonging to thin-layer electrodeposition topic.

The main result of our simulations is a qualitative one and consists in the resemblance of the calculated temperature profiles along the cell and the corresponding profiles obtained experimentally in [4]. The features of the calculated profiles are the same for all the values of the parameters we have used and this means that the temperature distribution along the cell is due to the specific structure in four regions of an ECD cell. The temperature increases obtained in our calculations are smaller than those measured and reported in [4]. This is not surprising because our model is a very simplified version of the real world: we have not considered the growth process, the transport by diffusion and convection, and any other heat generation process than the ohmic heating. It is a real challenge to include in a model what is missing in the simulation we have performed until now but the work is in progress. Even with our very simple model we have obtained some new results: the temperature profile *T(x)* in the direction parallel with the growing front, the shift of the temperature maximum position in 3D cell, and the dependencies of *T(y)* and *T(x)* profiles on various parameters involved in the calculation. The confirmation of these results using more sophisticated models may have some implications on the experimental interpretation of concentration, flow, thermal and electrical measurements performed in such systems. All these will also help in future studies devoted to the ohmic effects on morphology selection in thin layer electrochemical deposition.

**Acknowledgments**

The author is thankful to PDE Solutions Inc. for providing the student version of the FlexPDE solver.

## References

[1] J. Newman, Electrochemical Systems, J.Wiley & Sons, New York (2004).
[2] F. Sagues, M. Q. Lopez-Salvans & J. Claret, Physics Reports **337**, 97 (2000).
[3] D. P. Barkey, D. Watt, Z.Liu & S.Raber, J. Electrochem. Soc.**141**, 1206 (1994).
[4] M. Schrötter, K. Kassner, I. Rehberg, J. Claret & F. Sagues, Phys.Rev. E **66**, 026307 (2002).
[5] C. Leger, J. Elezgaray & F. Argoul, Phys. Rev. E **61**, 5452 (2000) and references therein.
[6] P. Barvinschi, Analele Universitatii de Vest din Timisoara, Seria Fizica, **45**, 158 (2004).
[7] D. Dobos, Electrochemical Data, Elsevier, New York (1975).
[8] R. C .Weast (Ed.), CRC Handbook of Chemistry and Physics, CRC Press Inc., (1977).
[9] J. -N. Chazalviel, Phys. Rev. A **42**, 7355 (1990).
[10] PDE Solutions Inc. USA; www.pdesolutions.com.
[11] F. White, Heat and Mass Transfer, Addison-Wesley Publishing Company, Reading, Massachusetts (1988).

*Corresponding author: pbarvi@physics.uvt.ro